Ultrasound Bone Segmentation Using Dynamic Programming

Pezhman Foroughi*, Emad Boctor*, Michael J. Swartz†, Russell H. Taylor*, and Gabor Fichtinger*‡
*Computer Science Department, Johns Hopkins University, Baltimore, USA
†Radiation Oncology and Molecular Radiation Sciences, Johns Hopkins University, Baltimore, USA
‡School of Computing, Queen's University, Kingston, Canada

***Abstract*—Segmentation of bone surface in ultrasound images has numerous applications in computer aided orthopedic surgery. A robust bone surface extraction technique for ultrasound images can be used to non-invasively probe the bone surface. In this work, we present early results with an intuitive and computationally inexpensive bone segmentation approach. The prior knowledge about the appearance of bone in ultrasound images is exploited toward achieving robust and fast bone segmentation. Continuity and smoothness of the bone surface are incorporated in a cost function, which is globally minimized using dynamic programming. The performance of this method is evaluated on ultrasound images collected from two male cadavers. The images are segmented in about half a second making the algorithm suitable for real-time applications. Comparison between manual and automatic segmentation shows an average accuracy of less than 3 pixels (0.3 mm).**

I. Introduction

The application of ultrasound in Computer Assisted Orthopedic Surgery (CAOS) has been limited due to poor quality of bone appearance in ultrasound compared to CT/MR. Nonlinear characteristics of ultrasound, low signal-to-noise ratio, speckles, and reverberations make it exceedingly difficult to accurately and reliably determine the bone surface.

In CAOS, ultrasound bone segmentation is mostly employed to collect sample points from the bone [1] or to extract the full 3D bone surface [2], which can be used for registration to other modalities specially pre-operative CT. Segmentation of scaphoid for percutaneous pinning [1], femur and pelvis [3], [4] are a few examples. In these applications, segmentation is usually carried out manually or semi-automatically. Since a large number of ultrasound images can be collected in a matter of seconds, manual segmentation is extremely time-consuming and might limit the number of the images that can be processed. A fast and robust segmentation overcomes such limitations.

As discussed in [5], exploiting the knowledge about the physics of ultrasound has proved to be successful for segmentation tasks. The bony anatomy creates a specific response in the B-mode ultrasound images [6]. High reflection and shadowing effect are two of the well-known and prominent features that are mainly utilized for this purpose.

In this paper, we exploit the prior knowledge about the appearance of bone in ultrasound images toward achieving robust and fast bone segmentation. For each pixel, the probability of being on the surface of bone is calculated by a score combining effects of both the shadow under the bone and reflection on the surface of the bone. The shadow is modeled as the sum of the pixel intensities in the shadow region weighted by a Gaussian function. The reflection effect manifests itself in high pixel intensity where the surface is near perpendicular to the direction of propagation of the ultrasound wave. The product of scores thus computed for shadowing and intensity is used as probability of being a bone surface pixel. A binary threshold mask excludes the parts of the image that are considered not to be bone, thereby increases the speed of the algorithm.

A cost function incorporating continuity and smoothness is then "globally" minimized using dynamic programming which is fast and eliminates the threat of local minima. This function determines where the bone starts and ends in the images as well. It is assumed that for each scan line, there is at most one pixel representing the bone surface.

Although the algorithm is introduced as a "hard segmentation", which results in a binary output, "soft segmentation" can be achieved by updating the bone probability map with this binary outcome.

II. Method

Our segmentation method involves two major steps. First, the bone surface is enhanced in the ultrasound image using the image intensities and the shadow effect. A number between 0 and 1 is calculated and assigned to each pixel. This number is interpreted as the probability of being on the surface of the bone. In the next step, dynamic programming is employed to minimize a cost function. This cost function determines the existence of the bone in the image and its location.

To increase the speed, the pixels with very low intensity values (lower than 0.125) are not processed. A binary mask is computed from the smoothed ultrasound image for this purpose. The mask also excludes 2 mm of the top part of the image. In this area, the bone cannot be reliably detected since it is very close to the ultrasound transducer. Basically, the thickness of the soft tissue between the bone and the transducer is required to be more than 2 mm.

The bone surface creates a strong reflection where the surface is near perpendicular to the direction of the ultrasound wave. This reflection appears as a bright ridge with some thickness [6]. Therefore, the pixels that belong to stripes of high intensity have larger probability to be on the bone surface. To model this, the Laplacian of Gaussian (LoG) of the

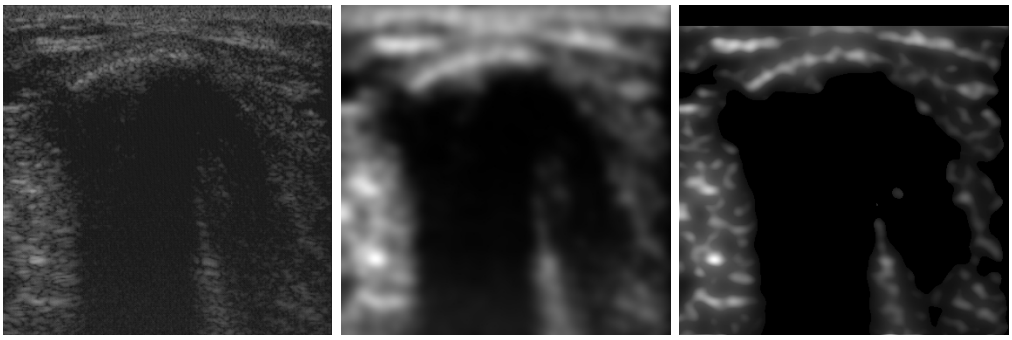

(a) Ultrasound image (b) Blurred image (c) Reflection number

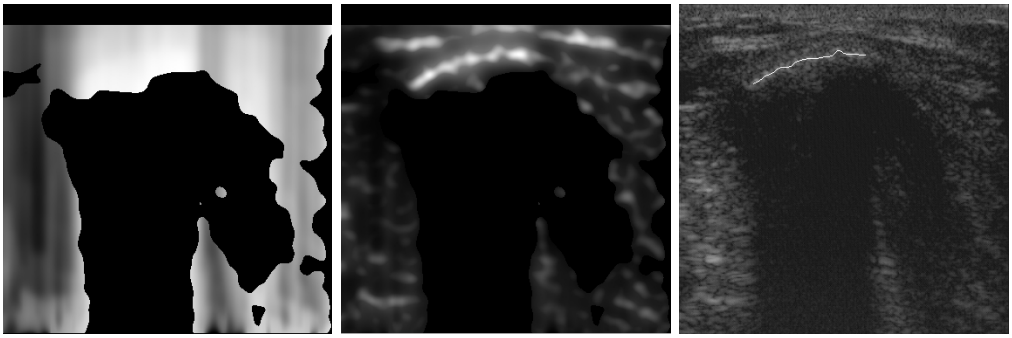

(d) Shadow value (e) Bone probability (f) Segmented image

Fig. 1. Intermediate images of the segmentation algorithm. A binary mask is applied to c),d) and e) excluding the very low intensity values and 2 mm of the top part of the images.

ultrasound image is calculated. Since only negative values of LoG are of our interest, the positive values are set to zero, and the rest is negated. This is then added to the blurred version of the image, and the result, referred to as the "reflection number", is normalized between zero and one (see Figures 1(b) and 1(c)).

Another feature caused by bone surface in addition to strong reflection is the shadow effect. Due to large impedance mismatch, a very small portion of ultrasound energy passes through the bone surface. Hence, the area beneath the bone appears to be dark in the ultrasound image. The bone shadow is known to be one of the most invariant features available [4] and is the key to distinguish between the bone surface and other high intensity ridges.

The shadow below a pixel is quantified by weighted summation of the intensity values of all pixels beneath as follows:

$$SH(p(a,b)) = \frac{\sum_{j=b}^{H} G(j-b)I(a,j)}{\sum_{j=b}^{H} G(j-b)}, \qquad (1)$$

where $SH(p(a,b))$ is the shadow value for pixel p at row a and scan line b of the image. H indicates the number of rows in the image. $G(.)$ and $I(.)$ represent the Gaussian weighting function and pixel intensity respectively. The Gaussian weighting function models the transition of high intensity pixels close to bone surface to the dark pixels deeper under the bone. Figure 1(d) shows the shadow map calculated for the ultrasound image of Figure 1(a). In this Figure, high intensity represents a stronger shadow effect. As described before, the masked pixels are set to zero.

The shadow value is normalized, and its product with the reflection number is defined as the bone probability (assuming the independence of these values). Figure 1(e) depicts one example of the resulting image. It should be noted that any other metric or bone enhancement algorithm such as the one described in [7] could also be inserted for estimation of the bone probability.

It is assumed that for each scan line of ultrasound image, only one pixel is on the bone surface at maximum. In order to segment the bone surface, for each scan line, existence of the bone edge and its location should be determined. The goal of segmentation would be to find a path $C(s)$ parametrized by s that minimizes a cost function. The path may consist of up to three different regions namely the "bony" region, the "boneless" region, and the "jump" section as shown in Figure 2. Similar to the snakes, the cost function of each path consists of internal and external energy components. However, it is formulated in a recursive format as shown below which is suitable for dynamic programming minimization:

$$minC(i,j) = E_{int}(i,j) + \min_{k}\{minC(k,j-1) + E_{ext}(k,j)\}, \qquad (2)$$

where $minC(i,j)$ is the minimum cost of moving from first scan line to the jth scan line at ith row with E_{int} and E_{ext} representing the internal and external energies. The internal

energy, $E_{int}(i,j)$, is defined as one minus the bone probability. The internal energy selected for the "boneless" area acts as a threshold for the bone probability. The proper selection of this value and its effect on segmentation is discussed in Section III.

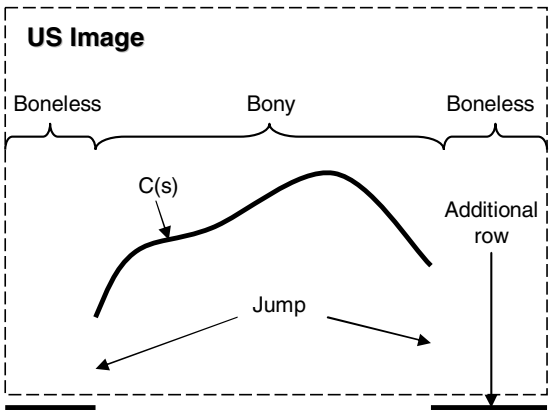

Fig. 2. The bone segmentation represented as a curve $C(s)$. The curve may consist of three parts: the bone surface ("bony" region); the area without bone ("boneless" region); and the "jump" between the two regions.

The external energy, E_{ext}, incorporates connectivity, and smoothness of the bony anatomy. The external energy is defined separately for each of the three portions of the segmentation path as follows:

$$E_{ext}(k,j) = \begin{cases} \alpha\|\frac{\mathrm{d}C}{\mathrm{d}s}\|^2 + \beta\|\frac{\mathrm{d}^2C}{\mathrm{d}s^2}\|^2 + \gamma & \text{if } \textit{bony} \\ JumpCost & \text{if } \textit{jumping} \\ \alpha D_1^2 + \beta D_2^2 & \text{if } \textit{boneless} \end{cases} \quad (3)$$

The constants, α and β, control the smoothness and curvature calculated from the first and the second derivative. γ is a small negative scalar and encourages larger connected bone curves by reducing the cost function. To further emphasize connectivity, frequent jumps between "bony" and "boneless" regions are penalized by the addition of the $JumpCost$ constant. For the "boneless" region, the first and second order derivatives are assigned to be constants D_1 and D_2 (in our implementation $D_1 = D_2 = 1$). This reduces the overall sensitivity of the algorithm to the parameters α and β.

For the dynamic programming optimization, the minimum index calculated from Equation (2) is recorded in an index matrix $minI(.)$ (*memoization*). The following equation illustrates the *memoization* step:

$$minI(i,j) = \arg\min_k \{minC(k,j-1) + E_{ext}(k,j)\}. \quad (4)$$

The last step of the optimization would be to trace back the optimal path from the last scan line as shown below:

$$C_{opt}(s) = \begin{cases} NB, & s = W \\ minI(s+1, C_{opt}(s+1)), & s = 1 \cdots W-1. \end{cases} \quad (5)$$

where C_{opt} is the computed optimal path, and NB is the index of an additional row (for example $H+1$) used for "boneless" region. The path start from and ends in this region. W indicates the number of scan lines.

This formulation yields global optimization only if the parameter β in Equation (3) is set to zero. This is because three consecutive samples of $C(s)$ are required in order to compute the second order derivative. However, the effect of the second derivative is local for a small β, and the optimal path would be close to a smoothed version of the "global" optimal path with $\beta = 0$.

The axial resolution of ultrasound images is much higher than the lateral resolution. The scan lines of B-mode ultrasound are normally interpolated inside the ultrasound system to construct a square pixel. In our implementation, the original number of scan lines are recovered approximately by downsampling the B-mode image in the axial direction in order to reduce extra processing of the interpolated data and increase the speed of optimization.

III. Results

Ultrasound images from two cadaver experiments were obtained to evaluate the segmentation. The images were collected using SonoSite portable ultrasound system with a high frequency transducer. B-mode images were digitized using a capture card connected to the s-video output of the ultrasound machine. The size of the images were 378x378 pixels where each pixel was a square with 0.1 mm side.

To construct a ground truth, the bone surfaces in 40 images were manually segmented using ANALYZE (Mayo Clinic, Rochester, Minn.). The automatic segmentation was then compared to the manual segmentation. Table I shows the results of the comparison with different threshold values. As described before, the images are not directly thresholded; instead, the threshold value (the internal energy selected for the "boneless" region) affects the cost function. A higher threshold value, decreases the cost of "boneless" path discouraging "bony" area, and vice versa. Therefore, with a very high value, the whole bone might remain undetected. The number of images in which no bone is detected, despite the presence of the bony anatomy in the image, is listed under "detection failure" column in Table I.

TABLE I
COMPARISON OF AUTOMATIC SEGMENTATION WITH MANUAL SEGMENTATION.

Threshold	Avg. Error (pixels)	False Positive Rate	False Negative Rate	Detection failure
0.40	2.67	9.23%	3.10%	0
0.45	2.63	6.30%	5.12%	0
0.50	2.60	4.76%	10.68%	0
0.55	2.62	2.95%	17.47%	3
0.60	2.51	1.40%	21.72%	13
0.65	2.10	1.36%	23.38%	28

The average error is computed for the overlapping region where both manual and automatic segmentations detected the bone surface. The table shows that the average error is almost

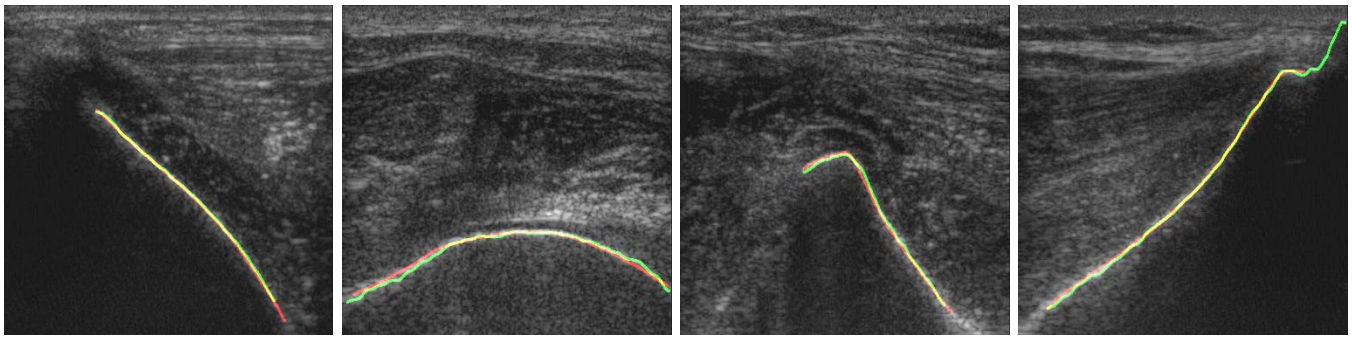

(a) (b) (c) (d)

Fig. 3. Segmentation results of ultrasound images obtained from pelvises and femurs of the cadavers. Red and green colors represent manual and automatic segmentation respectively. The segmentation lines are thickened for better visualization.

independent from the threshold value. This means that when the bone is correctly detected, the localization is accurate. False positive rate is defined as the width of the segment falsely detected as bone over the total width of bone from either manual or automatic segmentation. False negative rate is defined similarly.

Smaller false positive rate represents lower chance of outliers. This is important since usually lower number of outliers is favored specially for registration applications. However, very large threshold increases the false negative rate. The right value for the threshold should be selected based on the tolerance to the outliers. We have successfully used this algorithm (with the threshold value of 0.55) to extract bone surface sample points for an application where the extracted sample point are registered to pre-operative data.

Figure 3 shows the segmentation results for four ultrasound images. Red and green lines depict manual and automatic segmentation respectively. Figure 3(d) shows one example of disagreement between manual and automatic segmentation. Because of the strong shadow, the algorithm has extended the bone surface to the right which is not correct knowing the geometry of the scanned bone (pelvis in this case).

The algorithm is currently implemented in MATLAB, and the dynamic programming optimization is written as a MATLAB "mex" function. With this implementation, a 378x378 image is segmented in about 0.55 second. This time could be improved using code optimization and full C++ implementation.

IV. Conclusion and Future Work

In this paper, a bone segmentation method for ultrasound images was presented. The method can rapidly segment the bone surface in ultrasound images using bone features such as shadow effect and high intensity. The smoothness and continuity of the bone surface was incorporated in a cost function. Dynamic programming was used for fast optimization of the cost function. The algorithm was evaluated using ultrasound images obtained from two cadavers. The results of automatic segmentation was compared to manual segmentation. The preliminary results suggest that the accuracy and reliability of the segmentation is acceptable even when a high-end ultrasound machine is not used.

The segmentation can be improved in numerous ways including the addition of other bone enhancement metrics. It might be possible to incorporate the prior knowledge about the shape of the bony anatomy in the algorithm to reduce the chance of outliers. The speed of segmentation can also be improved by optimizing the code. In order to achieve a thorough conclusion on accuracy and robustness of algorithm using the comparison between manual and automatic segmentation, the variations of manual segmentation among different users should be studied. Finally, rigorous experiments are required for a complete validation of the method possibly using other ground truth alternatives.

Acknowledgment

The authors would like to thank Danny Song, MD and Hassan Rivaz for assisting in the cadaver experiments and Medtronic for loaning equipment. This work has been funded by National Science Foundation under EEC-9731478 and the William R. Kenan, JR Fund Award.

References

[1] M. Beek, P. Abolmaesumi, S. Luenam, R. Sellens, and D. Pichora, "Ultrasound-guided percutaneous scaphoid pinning: Operator variability and comparison with traditional fluoroscopic procedure," in *Medical Image Computing and Computer Assisted Intervention (MICCAI)*, 2006, pp. 536–543.

[2] Y. Zhang, R. N. Rohling, and D. K. Pai, "Direct surface extraction from 3D freehand ultrasound images," in *IEEE Visualization*, 2002, pp. 45–52.

[3] D. C. Barratt, G. P. Penney, C. S. K. Chan, M. Slomczykowski, T. J. Carter, P. J. Edwards, and D. J. Hawkes, "Self-calibrating ultrasound-to-CT bone registration," in *Medical Image Computing and Computer Assisted Intervention (MICCAI)*, 2005, pp. 605–612.

[4] D. V. Amin, T. Kanade, A. M. DiGioia, and B. Jaramaz, "Ultrasound registration of the bone surface for surgical navigation," *Computer Aided Surgery*, vol. 8, no. 1, pp. 1–16, 2003.

[5] J. A. Noble and D. Boukerroui, "Ultrasound image segmentation: A survey," *IEEE Transactions on Medical Imaging*, vol. 25, no. 8, pp. 987–1010, 2006.

[6] A. K. Jain and R. H. Taylor, "Understanding bone responses in b-mode ultrasound images and automatic bone surface extraction using a bayesian probabilistic framework," in *Proceedings of SPIE*, 2004, pp. 131–142.

[7] I. Hacihaliloglu, R. Abugharbieh, A. J. Hodgson, and R. N. Rohling, "Enhancement of bone surface visualization from 3D ultrasound based on local phase information," in *IEEE Ultrasonics Symposium*, October 2006, pp. 21–24.